

ous approaches can now be described as follows. In Fig. 4, A and C, the angle between the polariton wave vector and the  $z$  axis is fixed, but not its magnitude. In the absence of dispersion, this leads to a shock-wave singularity because of the constructive interference of waves of arbitrary  $q$ . In Fig. 4B, both the angle and  $q$  are predetermined because the components of  $\mathbf{q}$  orthogonal to  $\mathbf{e}_z$  are set by the grating. These considerations apply to the imaging experiments of (17) and to early work on polariton propagation (27) where the direction of motion can be identified with that of the Cherenkov expression. Finally, consider single-pump excitation when the source lateral dimensions are sufficiently large that the wave vectors of the pump pulse and the polariton are nearly collinear. In this case, the phase-matching condition is  $q \approx \Omega[n(\omega_L) + \omega_L n(\omega_L)]/c \equiv \Omega/c_g(\omega_L)$ . Because  $q \approx \Omega/c_0$  at low frequencies, it is clear that phase matching can only be attained at subluminal speeds, in agreement with Eq. 6; see Fig. 2C. Under the same (quasi-planar) conditions, and not too far from the pump pulse, the field for the grating method results from the interference between two polaritons at, say,  $q_x = \pm 2\pi/\ell$  and  $q_y = 0$ , where  $\ell$  is the grating spacing (12–17). This and Eq. 7 give  $q_z \ell = 2\pi(n^2 v^2/c^2 - 1)^{-1/2}$ , leading to  $E \sim \sin(2\pi x/\ell) \sin[q_z(z - vt)]$ . This field is represented in Fig. 4B by the rectangle with the checkerboard pattern (28).

References and Notes

1. V. P. Zrelov, *Cherenkov Radiation in High-Energy Physics* (Israel Program for Scientific Translations, Jerusalem, 1970).
2. T. Ypsilantis, J. Seguinot, *Nucl. Instrum. Methods A* **433**, 1 (1999), and references therein.
3. P. A. Cherenkov, *Dokl. Akad. Nauk SSSR* **2**, 451 (1934).
4. S. Vavilov, *Dokl. Akad. Nauk SSSR* **2**, 457 (1934).
5. I. Frank, *Vavilov-Cherenkov Radiation* (Nauka, Moscow, 1988).
6. \_\_\_\_\_, I. Tamm, *Dokl. Akad. Nauk SSSR* **14**, 109 (1937).
7. Expressions for the Cherenkov field in dispersive media were first derived by I. Tamm [*J. Phys.* **1**, 439 (1939)] and independently by E. Fermi [*Phys. Rev.* **57**, 485 (1940)], who used the Lorentz (single-pole) approximation to show that polarization effects lead to a reduction in the energy loss, a phenomenon known as the density effect. Ignoring dissipation, the condition for Cherenkov emission reads  $v^2 > c^2/\epsilon(\Omega)$ . Because  $\epsilon(\Omega)$  can reach large values in the proximity of a resonance, a particle can in principle radiate at arbitrarily small velocities.
8. G. N. Afanasiev, V. G. Kartavenko, E. N. Magar, *Physica B* **269**, 95 (1999), and references therein. This work was motivated in part by recent CR experiments with CERN's high-energy beam of lead ions (29, 30).
9. To the best of our knowledge, the numerical study of Afanasiev *et al.* (8) was the first to uncover differences between superluminal and subluminal CR. In their work, these differences manifest themselves in the separate open ( $v > c_0$ ) and closed ( $v < c_0$ ) behavior of the surfaces at which the field exhibits maxima.
10. D. H. Auston, K. P. Cheung, J. A. Valdmanis, D. A. Kleinman, *Phys. Rev. Lett.* **53**, 1555 (1984), and references therein.
11. D. A. Kleinman, D. H. Auston, *IEEE J. Quantum Electron.* **QE-20**, 964 (1984).
12. P. Grenier, D. Houde, S. Jandl, L. A. Boatner, *Phys. Rev. B* **50**, 16295 (1994).

13. O. Albert, C. A. Gautier, J. C. Loulergue, J. Etchepare, *Solid State Commun.* **107**, 567 (1998).
14. H. J. Bakker, S. Hunsche, H. Kurz, *Rev. Mod. Phys.* **70**, 523 (1998), and references therein.
15. G. P. Wiederrecht *et al.*, *Phys. Rev. B* **51**, 916 (1995).
16. H. P. Perry, T. P. Dougherty, *Phys. Rev. B* **55**, 5778 (1997).
17. R. M. Koehl, S. Adachi, K. A. Nelson, *J. Chem. Phys.* **110**, 1317 (1999).
18. The calculations were performed with MATHEMATICA Version 4.0 (Wolfram Research, Inc., Champaign, IL, 1999).
19. The two regimes differ in that  $\mathbf{E} \equiv 0$  outside the cone for the superluminal case, whereas, for  $v < c_0$ , the intensity does not vanish notwithstanding a substantial drop at the boundary. Hence, there is a shock-wave singularity at superluminal but not at subluminal speeds. The presence of a cone (as opposed to a plane) at  $v < c_0$  contradicts the phase-velocity argument predicting  $\theta_c = 0$  because  $c/nv$  can be arbitrarily close to unity.
20. Unlike the superluminal case, in which  $\theta_c \leq \cos^{-1}(1/n_0)$ , the Cherenkov angle for  $v < c_0$  goes all the way to  $\theta_c = \pi/2$  at  $v = 0$ . Also note that  $ds/d\Omega \rightarrow \infty$  at  $\Omega = \Omega_c, \Omega_0$ , which, according to Eq. 4, leads to  $\alpha = 0$ . Hence, at subluminal speeds, radiation at these frequencies is concentrated at  $\rho = 0$ .
21. See, e.g., Y. R. Shen, *The Principles of Nonlinear Optics* (Wiley, New York, 1984). Materials with infrared-active vibrations, such as ZnSe, show an additional contribution to the nonlinear polarization due to the combined phonon-photon character of the eigenmodes. The energy density becomes  $-\sum \mathcal{E}_i \mathcal{E}_k (\chi_{ikm}^{(2)} E_m + R_{ik}^{(m)} Q_m)$ , where  $\mathcal{E}_k$  and  $E_m$  are electric field components of the pump pulse and that of the infrared radiation,  $Q_m$  is the amplitude of a phonon component, and  $R^{(m)}$  is its associated Raman tensor.
22. H. Li, *J. Phys. Chem. Ref. Data* **13**, 102 (1984).
23. Values of the infrared constants of ZnSe from the literature exhibit considerable scattering. Those in Fig. 2 were interpolated from measurements at 80 K (22) and at 2 K [A. Göbel, T. Ruf, J. M. Zhang, R. Lauck, M. Cardona, *Phys. Rev. B* **59**, 2749 (1999); T. Hattori, Y. Homma, A. Mitsuishi, M. Tacke, *Opt. Commun.* **7**,

- 229 (1973)]. Data for  $n$  in the visible range are available at temperatures above 90 K (22). Values at 10 K were obtained from an expression giving  $n(\Omega)$  in terms of the band gap, the carrier effective masses, and the value of  $n$  at the gap [B. Jensen, A. Torabi, *Infrared Phys.* **23**, 359 (1983)]. The latter was used as an adjustable parameter to fit the time-domain data.
24. T. E. Stevens, thesis, University of Michigan, Ann Arbor (2000).
25. M. Born, K. Huang, *Dynamical Theory of Crystal Lattices* (Clarendon, Oxford, 1996), p. 100.
26. We used heterodyne detection methods. The pump beam was modulated with a mechanical chopper at 3.51 kHz. The transmitted probe light was analyzed with a polarizing beam cube and spectrally resolved (24). The probe beam and a reference beam, also dispersed by the spectrometer, were focused onto separate photodiodes, and their voltage difference was measured with a dual channel EG&G 5320 digital lock-in amplifier to get  $\Delta t$ .
27. G. M. Gale, F. Vallée, C. Flytzanis, *Phys. Rev. Lett.* **57**, 1867 (1986).
28. In (14), pump-probe data for polaritons generated with a traveling grating were interpreted in terms of avoided mode crossings and anharmonicity. Given that Cherenkov field profiles can be fairly complicated, there may be a need to compare the experiments with calculations of the field due to a finite traveling grating before such interpretations can be accepted.
29. V. P. Zrelov, J. Ruzicka, A. A. Tyapkin, *JINR Rapid Commun.* **1[87-98]**, 23 (1998).
30. V. P. Zrelov, J. Ruzicka, A. A. Tyapkin, *CERN Courier* **38** (no. 9), 7 (1998)].
31. We are grateful to C. Aku-Leh for assistance with the calculations and to D. G. Steel for critical reading of the manuscript. T.E.S. would like to thank the Max-Planck-Institut für Festkörpertorschung for warm hospitality. Work supported by the NSF under grant DMR 9876862 and by the Air Force Office of Scientific Research under contract F49620-00-1-0328 through the Multidisciplinary University Research Initiative program.

29 September 2000; accepted 30 November 2000

# Directed Assembly of One-Dimensional Nanostructures into Functional Networks

Yu Huang,<sup>1\*</sup> Xiangfeng Duan,<sup>1\*</sup> Qingqiao Wei,<sup>1</sup> Charles M. Lieber<sup>1,2,†</sup>

One-dimensional nanostructures, such as nanowires and nanotubes, represent the smallest dimension for efficient transport of electrons and excitons and thus are ideal building blocks for hierarchical assembly of functional nanoscale electronic and photonic structures. We report an approach for the hierarchical assembly of one-dimensional nanostructures into well-defined functional networks. We show that nanowires can be assembled into parallel arrays with control of the average separation and, by combining fluidic alignment with surface-patterning techniques, that it is also possible to control periodicity. In addition, complex crossed nanowire arrays can be prepared with layer-by-layer assembly with different flow directions for sequential steps. Transport studies show that the crossed nanowire arrays form electrically conducting networks, with individually addressable device function at each cross point.

Nanoscale materials, for example, nanoclusters and nanowires (NWs), represent attractive building blocks for hierarchical assembly of functional nanoscale devices that could overcome fundamental and economic limitations of conventional lithography-based fab-

rication (1–4). Research focused on zero-dimensional nanoclusters has led to substantial advances, including the assembly of arrays with order extending from nanometer to micrometer length scales (4–9). In contrast, the assembly of one-dimensional (1D) nano-

## REPORTS

structures, such as NWs and carbon nanotubes (NTs), has met with much less success (10–12), although these materials offer great potential as building blocks for applications in nanoelectronics (1–3, 13–16) and photonics (17).

To achieve the substantial potential of NWs and NTs in these and other areas of nanotechnology will require the controlled and predictable assembly of well-ordered structures. We report an approach for the hierarchical assembly of 1D nanostructures whereby NWs are aligned in fluid flows with the separation and spatial location readily controlled. Crossed NW arrays were also prepared with layer-by-layer assembly with different flow directions for sequential steps. Transport studies show that the crossed NW arrays form electrically conducting networks, with individually addressable device function at each NW-NW cross point. This approach can be potentially used for organizing other 1D nanostructures into highly integrated device arrays and thus offers a general pathway for bottom-up assembly of new electronic and photonic nanosystems.

The gallium phosphide (GaP), indium phosphide (InP), and silicon (Si) NWs used in these studies were synthesized by laser-assisted catalytic growth (1, 18, 19) and subsequently suspended in ethanol solution. In general, we assembled arrays of NWs by passing suspensions of the NWs through fluidic channel structures formed between a poly(dimethylsiloxane) (PDMS) mold (20) and a flat substrate (Fig. 1). Parallel and crossed arrays of NWs can be readily achieved with single (Fig. 1A) and sequential crossed (Fig. 1B) flows, respectively, for the assembly process as described below.

A typical example of parallel assembly of NWs (Fig. 2A) shows that virtually all the NWs are aligned along one direction, i.e., the flow direction. There are also some small deviations with respect to the flow direction, which we will discuss below. Examination of the assembled NWs on larger length scales (Fig. 2B) shows that the alignment readily extends over hundreds of micrometers. Indeed, alignment of the NWs has been found to extend up to millimeter length scales and seems to be limited by the size of the fluidic channels, on the basis of experiments carried out with channels with widths ranging from 50 to 500  $\mu\text{m}$  and lengths from 6 to 20 mm.

We carried out several types of experiments to understand factors controlling the

alignment and average separation of the NWs. First, we find that the degree of alignment can be controlled by the flow rate. With increasing flow rates, the width of the NW angular distribution with respect to the flow direction (e.g., inset in Fig. 2C) substantially narrows. Comparison of the distribution widths measured over a range of conditions shows that the width decreases quickly from our lowest flow rate,  $\sim 4$  mm/s, and approaches a nearly constant value at  $\sim 10$  mm/s (Fig. 2C). At the highest flow rates examined in our studies, more than 80% of the NWs are aligned within  $\pm 5^\circ$  of the flow

direction (inset, Fig. 2C). Our observed results can be explained within the framework of shear flow (21, 22). Specifically, the channel flow near the substrate surface resembles a shear flow and aligns the NWs in the flow direction before they are immobilized on the substrate. Higher flow rates produce larger shear forces and hence lead to better alignment.

In addition, the average NW surface coverage can be controlled by the flow duration (Fig. 2D). Experiments carried out at a constant flow rate show that the NW density increases systematically with flow duration.

**Fig. 1.** Schematic of fluidic channel structures for flow assembly. (A) A channel formed when the PDMS mold was brought in contact with a flat substrate. NW assembly was carried out by flowing an NW suspension inside the channel with a controlled flow rate for a set duration. Parallel arrays of NWs are observed in the flow direction on the substrate when the PDMS mold is removed. (B) Multiple crossed NW arrays can be obtained by changing the flow direction sequentially in a layer-by-layer assembly process.

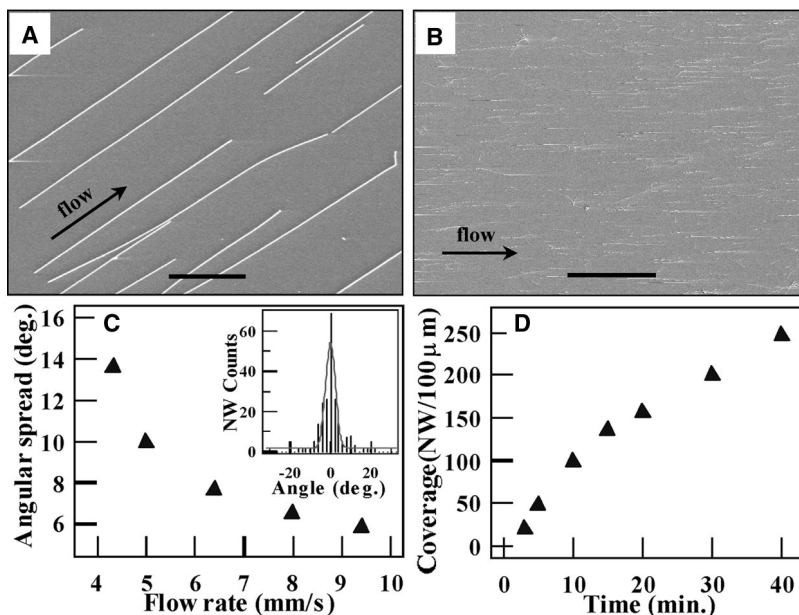
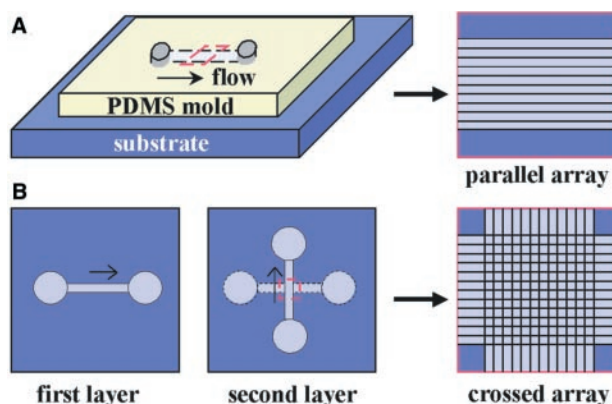


**Fig. 2.** Parallel assembly of NW arrays. (A and B) SEM images of parallel arrays of InP NWs aligned by channel flow. The scale bars correspond to 2  $\mu\text{m}$  in (A) and 50  $\mu\text{m}$  in (B), respectively. The silicon ( $\text{SiO}_2/\text{Si}$ ) substrate used in flow assembly was functionalized with an  $\text{NH}_2$ -terminated self-assembled monolayer (SAM) by immersion in a 1 mM chloroform solution of 3-aminopropyltriethoxysilane (APTES) for 30 min, followed by heating at  $110^\circ\text{C}$  for 10 min (10). All of the substrates used in the following experiment were functionalized in a similar way unless otherwise specified. (C) NW angular spread with respect to the flow direction versus flow rate. Each data point in the figure was obtained by statistical analysis of angular distribution of  $\sim 200$  NWs (e.g., see inset). The inset shows a histogram of NW angular distribution at a flow rate of 9.40 mm/s. (D) The average density of NWs versus flow time. The average density was calculated by dividing the average number of NWs at any cross section of the channel by the width of the channel. All of the experiments were carried out with a flow rate of 6.40 mm/s.

<sup>1</sup>Department of Chemistry and Chemical Biology, Harvard University, Cambridge, MA 02138, USA. <sup>2</sup>Division of Engineering and Applied Sciences, Harvard University, Cambridge, MA 02138, USA.

\*These authors contributed equally to this work.

†To whom correspondence should be addressed. E-mail: cml@cmliris.harvard.edu

In these experiments, a flow duration of 30 min produced a density of about 250 NWs per 100  $\mu\text{m}$  or an average NW-NW separation of  $\sim 400$  nm. Extended deposition time can produce NW arrays with spacings on the

order of 100 nm or less. We note that the deposition rate and hence average separation versus time depend strongly on the surface chemical functionality. Specifically, we show that the GaP, InP, and Si NWs deposit more

rapidly on  $\text{NH}_2$ -terminated monolayers, which have a partial positive charge, than on either methyl-terminated monolayers or bare  $\text{SiO}_2$  surfaces. It is also important to recognize that the minimum separation of aligned NWs that can be achieved without NW-NW contacts will depend on the lengths of the NWs used in the assembly process. Recent progress demonstrating control of NW lengths from the 100-nm to tens-of-micrometer scale (23) should increase the range of accessible spacings without contact.

Our results demonstrate ordering of NW structure over multiple length scales—organization of nanometer diameter wires with 100-nm to micrometer-scale separations over millimeter-scale areas. This hierarchical order can readily bridge the microscopic and macroscopic worlds, although to enable assembly with greatest control requires that the spatial position also be defined. We achieved this important goal by using complementary chemical interactions between chemically patterned substrates and NWs (Fig. 3A). Scanning electron microscopy (SEM) images of representative experiments (Fig. 3, B to D) show parallel NW arrays with lateral periods the same as those of the surface patterns. These data demonstrate that the NWs are preferentially assembled at positions defined by the chemical pattern and, moreover, show that the periodic patterns can organize the NWs into a regular superstructure. It is important to recognize that the patterned surface alone does not provide good control of the 1D nanostructure organization. Assembly of NTs (10, 11) and NWs (24) on patterned substrates shows 1D nanostructures aligned with, bridging, and looping around patterned areas with little directional control. Our use of fluid flows avoids these substantial problems and enables controlled assembly in one or more directions. By combining this approach with other surface-patterning methods, such as nanoscale domain formation in diblock copolymers (25) and spontaneous ordering of molecules (26), it should be possible to generate well-ordered NW arrays beyond the limitations of conventional lithography.

Our general approach can be used to organize NWs into more complex crossed structures, which are critical for building dense nanodevice arrays, with the use of the layer-by-layer scheme illustrated in Fig. 1B. The formation of crossed and more complex structures requires that the nanostructure-substrate interaction is sufficiently strong that sequential flow steps do not affect preceding ones: We find that this condition can be achieved. For example, alternating the flow in orthogonal directions in a two-step assembly process yields crossbar structures (Fig. 4, A and B). Both figures show that multiple crossbars can be obtained with only hundreds of nanometer separations between individual

**Fig. 3.** Assembly of periodic NW arrays. (A) Schematic view of the assembly of NWs onto a chemically patterned substrate. The light gray areas correspond to  $\text{NH}_2$ -terminated surfaces, whereas the dark gray areas correspond to either methyl-terminated or bare surfaces. NWs are preferentially attracted to the  $\text{NH}_2$ -terminated regions of the surface. (B and C) Parallel arrays of GaP NWs aligned on poly(methyl methacrylate) (PMMA) patterned surface with 5- and 2- $\mu\text{m}$  separation. The dark regions in the image correspond to residual PMMA, whereas the bright regions correspond to the  $\text{NH}_2$ -terminated  $\text{SiO}_2/\text{Si}$  surface. The NWs are preferentially attracted to  $\text{NH}_2$ -terminated regions. The PMMA was patterned with standard electron beam (E-beam) lithography, and the resulting  $\text{SiO}_2$  surface was functionalized by immersion in a solution of 0.5% APTES in ethanol for 10 min, followed by 10 min at 100°C. The scale bars correspond to 5  $\mu\text{m}$  and 2  $\mu\text{m}$  in (B) and (C), respectively. (D) Parallel arrays of GaP NWs with 500-nm separation obtained with a patterned SAM surface. The  $\text{SiO}_2/\text{Si}$  surface was first functionalized with methyl-terminated SAM by immersion in pure hexamethyldisilazane (HMDS) for 15 min at 50°C, followed by 10 min at 110°C. This surface was patterned by E-beam lithography to form an array of parallel features with a 500-nm period, followed by functionalization with APTES (70). The scale bar corresponds to 500 nm.

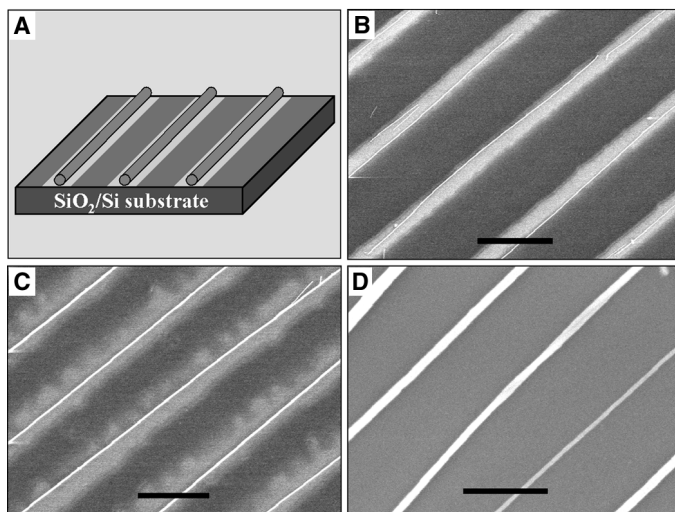
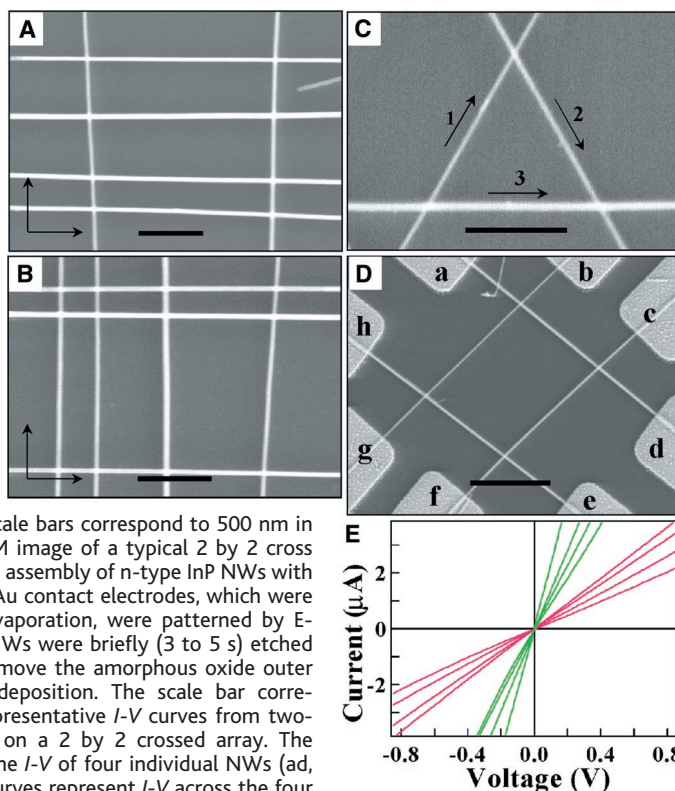


**Fig. 4.** Layer-by-layer assembly and transport measurements of crossed NW arrays. (A and B) Typical SEM images of crossed arrays of InP NWs obtained in a two-step assembly process with orthogonal flow directions for the sequential steps. Flow directions are highlighted by arrows in the images. (C) An equilateral triangle of GaP NWs obtained in a three-step assembly process, with 60° angles between flow directions, which are indicated by numbered arrows. The scale bars correspond to 500 nm in (A), (B), and (C). (D) SEM image of a typical 2 by 2 cross array made by sequential assembly of n-type InP NWs with orthogonal flows. Ni/In/Au contact electrodes, which were deposited by thermal evaporation, were patterned by E-beam lithography. The NWs were briefly (3 to 5 s) etched in 6% HF solution to remove the amorphous oxide outer layer before electrode deposition. The scale bar corresponds to 2  $\mu\text{m}$ . (E) Representative  $I$ - $V$  curves from two-terminal measurements on a 2 by 2 crossed array. The green curves represent the  $I$ - $V$  of four individual NWs (ad, bg, cf, eh), and the red curves represent  $I$ - $V$  across the four n-n crossed junctions (ab, cd, ef, gh).



cross points in a very straightforward, low-cost, fast, and scalable process. Although the separations between individual NWs are not completely uniform, a periodic array can be easily envisioned with a patterned surface as described above. These crossbar structures can yield functional devices (see below).

We believe that our approach for directed assembly of multiple crossed NW arrays offers substantial advantages over current efforts, which have used random deposition (14, 16), direct manipulation of individual NWs and NTs (15), and electric fields (12, 16, 27) to make single crossed structures. With random deposition and manipulation, it is difficult to obtain multiple crossbars required for integrated nanodevices. Although electric fields enable more control over assembly, this method is also limited by (i) electrostatic interference between nearby electrodes as separations are scaled below the micrometer level and (ii) the requirement of extensive lithography to fabricate the electrodes for assembly of multiple NW device structures. Our fluidic approach is intrinsically very parallel and scalable and, moreover, it allows for the directed assembly of geometrically complex structures by simply controlling the angles between flow directions in sequential assembly steps. For example, an equilateral triangle (Fig. 4C) was assembled in a three-layer deposition sequence with 60° angles between the three flow directions. The method of flow alignment thus provides a flexible way to meet the requirements of many device configurations, including those requiring assembly of multiple "layers" of NWs.

An important feature of this layer-by-layer assembly scheme is that each layer is independent of the others, and thus a variety of homo- and heterojunction configurations can be obtained at each crossed point by simply changing the composition of the NW suspension used for each step. For example, it should be possible to directly assemble and subsequently address individual nanoscale devices using our approach with n-type and p-type NWs (16, 19) and NTs, in which the NWs and NTs act as both the wiring and active device elements (15). A typical 2 by 2 crossbar array made of n-type InP NWs, in which all eight ends of the NWs are connected by metal electrodes, demonstrates this point (Fig. 4D). Transport measurements (Fig. 4E) show that current can flow through any two of the eight ends and enable the electrical characteristics of individual NWs and the NW-NW junctions to be assessed. The current-voltage ( $I$ - $V$ ) data recorded for each of the four cross points exhibit linear or nearly linear behavior (red curves) and are consistent with expectations for n-n type junctions. Because single NW-NW p-n junctions formed by random deposition exhibit behavior characteristic of light-emitting diodes (LEDs) (16), we believe that our approach could be used to assemble high-density and individually addressable nano-

LEDs and electronically more complex nanodevices.

These studies provide a general and rational approach for hierarchical assembly of 1D nanomaterials into well-defined functional networks that can bridge the nanometer through millimeter size regimes. We have shown that NWs can be assembled into parallel arrays with control of the average separation and, by combining fluidic alignment with surface-patterning techniques, that it is also possible to control periodicity. In addition, we have demonstrated the possibility of layer-by-layer assembly of crossed and more complex structures by varying the flow direction in sequential steps and have obtained preliminary results suggesting that this approach can be extended to 1D nanostructures, such as carbon NTs (28). We believe that flow assembly represents a general strategy for organization of NW and NT building blocks into structures needed for wiring, interconnects, and functional devices and thus could enable a bottom-up manufacturing paradigm for future nanotechnologies.

References and Notes

1. J. Hu, T. W. Odom, C. M. Lieber, *Acc. Chem. Res.* **32**, 435 (1999).
2. C. Dekker, *Phys. Today* **52** (no. 5), 22 (1999).
3. J. R. Heath *et al.*, *Science* **280**, 1716 (1998).
4. C. A. Mirkin, *Inorg. Chem.* **39**, 2258 (2000).
5. C. B. Murray, C. R. Kagan, M. G. Bawendi, *Science* **270**, 1335 (1995).
6. C. P. Collier *et al.*, *Annu. Rev. Phys. Chem.* **49**, 371 (1998).

7. A. K. Boal *et al.*, *Nature* **404**, 746 (2000).
8. R. C. Hayward, D. A. Sayille, I. A. Aksay, *Nature* **404**, 56 (2000).
9. M. Li, H. Schnablegger, S. Mann, *Nature* **402**, 393 (1999).
10. J. Liu *et al.*, *Chem. Phys. Lett.* **303**, 125 (1999).
11. M. Burghard *et al.*, *Adv. Mater.* **10**, 584 (1998).
12. P. A. Smith *et al.*, *Appl. Phys. Lett.* **77**, 1399 (2000).
13. S. J. Tan *et al.*, *Nature* **393**, 49 (1998).
14. M. S. Fuher *et al.*, *Science* **288**, 494 (2000).
15. T. Rueckes *et al.*, *Science* **289**, 94 (2000).
16. X. Duan *et al.*, *Nature* **409**, 66 (2001).
17. S. Noda *et al.*, *Science* **289**, 604 (2000).
18. X. Duan, C. M. Lieber, *Adv. Mater.* **12**, 298 (2000).
19. Y. Cui, X. Duan, J. Hu, C. M. Lieber, *J. Phys. Chem. B* **104**, 5213 (2000).
20. D. C. Duffy *et al.*, *Anal. Chem.* **70**, 4974 (1998).
21. C. A. Stover, D. L. Koch, C. Cohen, *J. Fluid Mech.* **238**, 277 (1992).
22. D. L. Koch, E. S. G. Shaqfeh, *Phys. Fluids A* **2**, 2093 (1990).
23. We have shown that the NWs with well-defined and controllable lengths can be prepared using gold nanocluster catalysts (M. S. Gudiksen, J. Wang, C. M. Lieber, in preparation).
24. Y. Huang, X. Duan, C. M. Lieber, unpublished data.
25. C. De Rosa *et al.*, *Macromolecules* **33**, 4871 (2000).
26. M. Gleiche, L. F. Chi, H. Fuchs, *Nature* **403**, 173 (2000).
27. Electric fields can be used to align suspensions of semiconductor NWs into parallel NW arrays and single NW crosses (16), where patterned microelectrode arrays are used to create a field pattern. Fringing fields and charging can, however, lead to substantial complications in the assembly of multiple crosses at the submicrometer scale.
28. Additional studies show that suspensions of single-walled carbon nanotubes and duplex DNA can be aligned in parallel arrays with the fluidic approach.
29. We thank H. Stone, J. Ng, and T. Rueckes for helpful discussions. C.M.L. acknowledges support of this work by the Office of Naval Research and Defense Advanced Projects Research Agency.

10 October 2000; accepted 13 December 2000

## Fast Drop Movements Resulting from the Phase Change on a Gradient Surface

Susan Daniel, Manoj K. Chaudhury,\* John C. Chen

The movement of liquid drops on a surface with a radial surface tension gradient is described here. When saturated steam passes over a colder hydrophobic substrate, numerous water droplets nucleate and grow by coalescence with the surrounding drops. The merging droplets exhibit two-dimensional random motion somewhat like the Brownian movements of colloidal particles. When a surface tension gradient is designed into the substrate surface, the random movements of droplets are biased toward the more wettable side of the surface. Powered by the energies of coalescence and collimated by the forces of the chemical gradient, small drops (0.1 to 0.3 millimeter) display speeds that are hundreds to thousands of times faster than those of typical Marangoni flows. This effect has implications for passively enhancing heat transfer in heat exchangers and heat pipes.

The movements of liquids resulting from unbalanced surface tension forces constitute an important surface phenomenon, known as the Marangoni effect (1). When regulated properly, these types of flows are of value in several industrial applications, such as the design and operation of microfluidic and integrated DNA

analysis devices (2-4). Although the usual Marangoni motions are triggered by variations in temperature or composition on a liquid surface, a surface tension heterogeneity (5-7) on a solid substrate can also induce such motion. The typical speeds of these flows (speeds ranging from micrometers to millimeters per second) on a